

# Correlation between Phase Transition Properties and Lattice-dynamical Instabilities in Metallic Materials

Koji MORIGUCHI\*  
Yusaku TOMIO

Hidenori TERASAKI

## Abstract

*Phase transitions can be regarded as response phenomena in which a phase having certain characteristic stability and rigidity is broken against relatively large “external forces” such as heat, stress, chemical potential, and light. In this article, we report on the systematic investigation into correlations between the typical first-order phase transitions (such as melting and/or martensitic transformation) and the energetics as a function of lattice strains using the concepts of the Bain path, the physically allowed lattice-invariant (PALI) strain, and the generalized stacking fault (GSF) energy surface, within the framework of empirical potential and/or electronic structural descriptions. We discuss the conceptual relations of the first-order phase transition behaviors with elasticity, energetics, and lattice-dynamical instabilities found in our various atomistic simulations and show that the lattice-dynamical instabilities along these paths might also be useful information even for understanding the martensitic transformation in steel. In relation to these theoretical concepts, our in-situ experimental studies on the elastic moduli in steel alloys measured during the cooling cycle using the ultrasonic pulse sing-around method are also reported. The correlations between elastic modulus and austenite stability found in polycrystalline steel alloys are discussed based on the theoretical concepts above.*

## 1. Introduction

Regardless of engineering classifications such as structural or functional material, materials show response phenomena for various “external forces” or their changes such as heat, stress, chemical potential, light, and so on. Phase transition or phase transformation can be considered as a rigidity catastrophe where a phase of the physical state with characteristic stability and/or rigidity is broken to a relatively large degree against “external forces”.<sup>1,2)</sup> Since the critical point of phase transition is a quantitative index, which measures the phase stability for “external forces” of the phase concerned, it is an important physical property for the development of materials and/or processes. For example, the melting point, which is a physically important quantity in solidification phenomena, is often used as an index indicating the high temperature resistance qualitatively even in industrial solid materials.

In contrast, if the accurate simulations and/or computer controls on complicated metallographic changes during the thermomechanical treatments become possible, it will be easier to stably supply the products with minimum total cost that satisfy the customers. Therefore, the material prediction technology using computers is highly expected. For example, since the mesoscopic dynamical simulations based on the Ginzburg-Landau type theory represented by the Phase-Field (PF) method are considered to be promising not only for essentially understanding non-equilibrium phenomena mediated by external forces, but also for the theoretical frameworks to describe the traditional experimental findings,<sup>3,4)</sup> their applications have been used for various fields in Nippon Steel & Sumitomo Metal Corporation.<sup>5-10)</sup>

The mathematical framework of the PF method is positioned as the optimization problem for free energy functional spaces spanned

\* Chief Researcher, Dr.Eng., Mathematical Science & Technology Research Lab., Advanced Technology Research Laboratories  
20-1 Shintomi, Futtsu City, Chiba Pref. 293-8511

by some order parameters that have been artificially modelled in advance. In the framework of the PF method, various variables in the time evolution equations derived using the variational principle can be associated with the measured physical properties through the asymptotic solution analyses.<sup>4)</sup> Since the multiple time evolution equations are essentially considered within the scheme, many competition phenomena are naturally observed within the PF method. For example, the method can reasonably describe the Mullins-Sekerka instabilities and the dynamic supercooling phenomena induced by the shape effects on the transition points and the interfacial movement speeds (i.e. Gibbs-Thomson effect and/or Laplace effect) during the phase transformation phenomena.<sup>4)</sup> In the free energy density space under consideration of the PF method, very interesting physical information on the phase transition is inherently found from the viewpoint of microscopic theory, while response phenomena other than the relaxation processes anticipated in the modeling are sometimes actually revealed.<sup>1,2)</sup>

In the melting phenomenon (solid-liquid phase transition) as a typical first order phase transition, the basic scientific problem of “what is the essence of solid-state melting” is present even currently. In order to solve this problem, focusing on the physical properties of the solid phase prior to melting (the initial phase of reaction), the theoretical approaches for the essence based on the solid state physics can date back to the works of Lindemann<sup>11)</sup> and Born<sup>12)</sup> at the beginning of the previous century. They have proposed the concepts for solid-liquid phase transition phenomena called the “Lindemann criterion” and the “Born criterion” similar to the concept of the “Ostwald’s Step Rule”,<sup>13)</sup> where the phase transitions can be regarded as successive reactions.

The former criterion by Lindemann proposes that the amplitude of atomistic vibrations in solids reaching a certain threshold results in melting phenomenon,<sup>11)</sup> and the latter by Born proposes that the elastic property of solids is relevant to the melting phenomenon and that the temperature at which the shear modulus and/or its anisotropy disappear corresponds to the melting point.<sup>12)</sup> These concepts including the physical principle to grasp the trends of material properties are also useful from the viewpoint of material design, since such concepts make it unnecessary to obviously obtain physical quantities such as transition temperatures that are difficult to derive directly.

In this article including the additional concepts and computational analyses not mentioned in Ref. 2), our microscopic theoretical studies on the phase transition will be reviewed,<sup>1,2)</sup> in which we have investigated the correlation between the thermodynamic stability and the lattice-dynamical instability in metallic crystal materials. In relation to these theoretical concepts, our *in-situ* experimental studies on the elastic properties in steel alloys measured during the martensitic transformation have also been reported.<sup>14–17)</sup>

## 2. Phase Stability and Lattice Strain Energetics in Metallic Materials

**Figure 1** shows a schematic energy diagram relevant to the reaction coordinate of phase transition. Phase transition is a typical cooperative phenomenon where the interactions among atoms and/or molecules in condensed phases act cooperatively to create new properties different from the properties in the isolated states. An abstract coordinate system describing its degree of progress along a reaction path is called the “reaction coordinate”. If an appropriate reaction coordinate describing the focused reaction and its relevant energy diagram are found in some way, we can discuss the relative stability of the initial status, the stability for external forces, the ri-

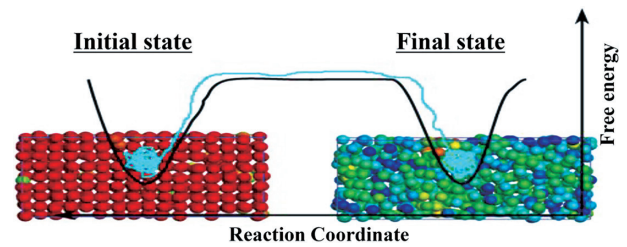


**Fig. 1** Schematic free-energy diagram as a function of reaction coordinate during phase-transition

The reaction path is not always comprehensible for the corresponding transition. If we find out the true reaction path as nearly as possible, the stability of initial state (or phase stability) can be estimated from the curves of free energy. The approximate curves of free energy near the initial state along the corresponding reaction coordinate might be described by the lattice strain energetics which represents the initial reaction for the transition.

gidity, the reaction speed, and so on, since the energy barrier on the reaction coordinate can be approximately estimated.

However, in the phase transition reaction which is a typical cooperative phenomenon, we often encounter difficulties that actual reaction coordinates are too complicated to understand in many cases or that it is not understood how the reaction coordinate system should be theoretically handled. The intrinsic importance of the works by Lindemann<sup>11)</sup> and Born<sup>12)</sup> described above has been to open up the route that can estimate the associated energy diagrams from only considering the initial states of reactions, in order to understand the unknown reaction coordinates. In this chapter, how the elasticity and/or more general framework of the strain energetics are linked to the thermodynamic properties in the crystalline materials from the microscopic view is discussed based on our theoretical studies.<sup>1,2)</sup>

### 2.1 Correlation between elastic property and phase stability in crystal lattices

In this section, we review the correlation between the elastic property that is a response phenomenon for infinitesimal strain and the thermodynamic phase stability.<sup>2)</sup> Since the first order phase transition generally changes the interatomic bonds in the focused phase to a greater or lesser extent, the phase stability of the phase is likely to depend on the strength of the interatomic bonds. In the systems with strong interatomic bonds, the total energy from the ground state steeply increases with respect to the distortion perturbation from the surroundings, so that the elastic constants as the resistance indices against the infinitesimal strain tend to increase in general. Therefore, it is intuitively assumed that some correlations are expected to appear between the elastic properties and the phase stability in crystal phases.

There have been many attempts to organize this kind of correlation from the measured values. For example, Fine et al. have pointed out that some linear relationships are found for the melting points  $T_M$  and the elastic constant  $C_{11}$  in many cubic metallic systems.<sup>18)</sup> Since the elastic constants for crystal lattices with small unit cells can now be easily evaluated using the first-principles calculations, we show the computational relationship between the elastic constants  $C_{11}$  and melting points  $T_M$  for the fcc lattices of some transition metals in **Fig. 2**. As pointed out by Fine et al., relatively good linear correlation can be seen in both values.<sup>2)</sup>

**Figure 3(a)** shows the structural energies for fcc and bcc in the 4d transition metal series using the first-principles calculations, in which the values are displayed using the energy increments from the

hcp structure for each element. The occupation number ( $n_d$ ) of d electrons plays an essential role in the relative stability of the crystal structure in the transition metal systems and the crystal structure in a ground state changes as hcp→bcc→hcp→fcc→hcp from the left side to the right in the periodic table (with the exception of the 3d transition metal systems that are also induced due to the magnetism). The canonical band analysis (i.e. the band-structure calculation excluding the individuality for nucleus) has also suggested that this structural transition behavior in the periodic table arises from the energy competition stability among lattices that stems from the boundary location between the bonding and anti-bonding states for the d bands.<sup>19)</sup>

Figure 3 (b) shows the calculation results of shear modulus  $C'$ (=

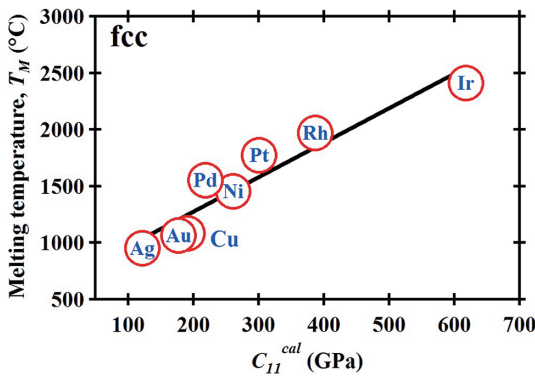


Fig. 2 Thermodynamic melting points ( $T_M$ ) as a function of  $C_{11}^{cal}$  for fcc transition metals  
The  $C_{11}^{cal}$  are evaluated using the first-principles calculations.<sup>2)</sup>

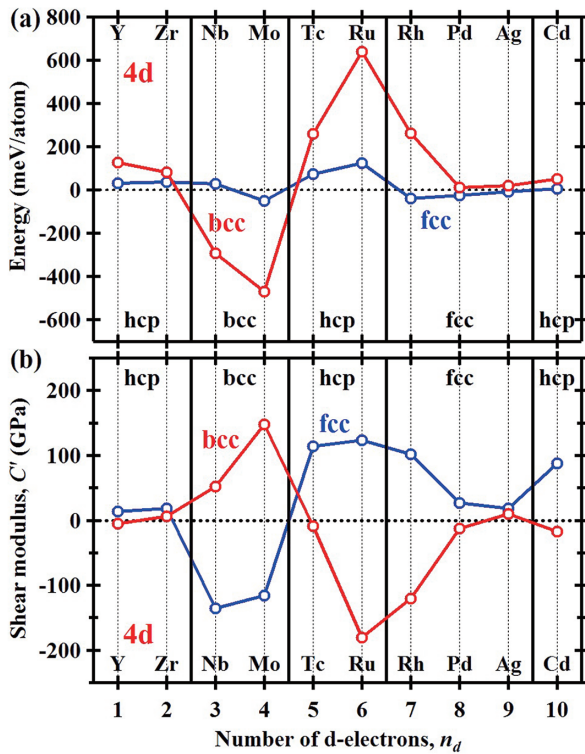


Fig. 3 (a) Lattice energy increments from hcp structure and (b) Shear moduli of  $C'=(C_{11}-C_{12})/2$  calculated for fcc and bcc in the 4d transition metals based on the first-principles calculations.<sup>2)</sup>

$(C_{11}-C_{12})/2$ ) for fcc and bcc lattices. The negative value of shear modulus in this figure physically means that the lattice-dynamical instability referred to as the elastic instability or the Born instability appears where the adiabatic potential curve due to the associated distortion is upwardly convex. If the bcc lattice is the thermodynamically most stable structure, the elastic instability of fcc (i.e. close-packed) lattice appears. In contrast, in the zone with fcc phase stability, we can find that the elastic instability of bcc appears. That is, the fcc and bcc lattices mutually conflict in the elastic instability. In this article, we call this elastic relation between bcc and fcc lattices a relationship of “conflicting lattices”. The reciprocity between bcc and fcc (close-packed lattice) described here is highly universal from various theoretical analyses.<sup>20,21)</sup> It can also be understood from the behavior of the energy curve on the Bain path deformation as described in detail in the next section. In this way, the phase stability of the crystal is closely related to the elastic property such as shear modulus and the detailed study on the elastic property can conversely lead to the essential understanding of the phase stability.

The phase stability of the solid phase such as the melting phenomenon on the high temperature side is also closely related to the shear modulus. Because the liquid phase has fluidity, it can be defined as “the phase losing shear modulus”. This is intuitively more understandable than the correlation between the crystal stability and elastic property described above. In Fig. 4, we show a typical example of the solid-liquid phase transition during the elevated temperature process by the molecular dynamics simulations based on the isobaric (NPT) ensemble using the AI-based Embedded Atom Method (EAM) potentials.<sup>1)</sup> Since the actual melting phenomenon is a typical phase transition triggered by the heterogeneous nucleation in the vicinity of the surface or of the defects, in the molecular dynamics simulations with the perfect crystal systems, considerable super-heating is usually observed, in which the melting transition cannot be induced at the thermodynamic melting point ( $T_M^t$ ).

At a certain temperature, the isotropic condition of vanishing shear moduli difference ( $C_{44}-C'=0$ ) is satisfied, and the discontinuity of the atomic volume can be observed. This temperature is called the mechanical melting point ( $T_M^m$ ), which corresponds to the limit

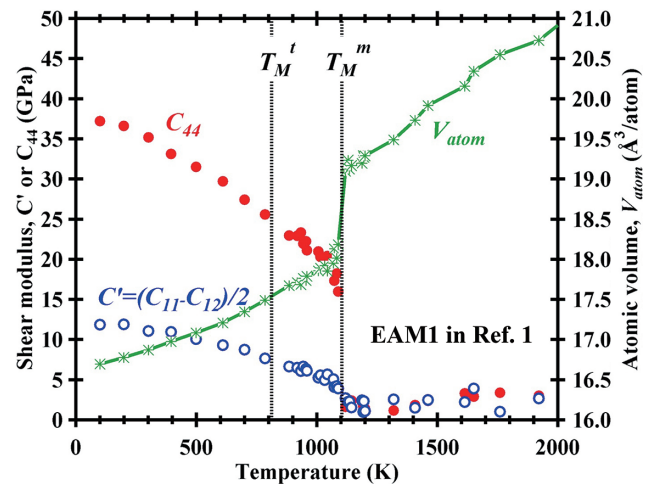


Fig. 4 Typical example of the temperature dependence of the atomic volume ( $V_{atom}$ ) and shear moduli ( $C'$  and  $C_{44}$ ) based on the NPT molecular-dynamics simulations based on the Embedded Atom Method.<sup>1)</sup>  
 $T_M^t$  and  $T_M^m$  denote the equilibrium (thermodynamic) and mechanical melting points, respectively.

temperature of the superheated state for the solid. More sophisticated MD simulations using the Lennard-Jones crystal have demonstrated the atomic-scale mechanisms of bulk melting and have shown that the Lindemann criterion<sup>11)</sup> and the Born criterion<sup>12)</sup> described in the preface are simultaneously satisfied at the mechanical melting point ( $T_M^m$ ).<sup>22)</sup> In the molecular dynamics analyses using some AI-based EAM potentials by the present authors, the strong linearity with considerable accuracy has been observed between the thermodynamic melting point  $T_M^t$  and the mechanical one  $T_M^m$ .<sup>1)</sup> Therefore, if the declining behavior of shear modulus during the elevated temperature does not depend on the substances, the phase stability of the crystal at high temperature is also suggested to have good correlation with the shear modulus.

## 2.2 Energetics of Bain and PALI strains: Phase stability and elastic instability among conflicting lattices

This section describes that the phase stability between fcc and bcc is closely related to the lattice dynamical instability called the elastic instability among the conflicting lattices, using the energetic concept for the Bain strain or the Physically Allowed Lattice-Invariant (PALI) strain.<sup>1,2)</sup>

Regarding the high-temperature phase stability in solids, some interesting findings have been reported from the materials-oriented aspects based on the first-principles calculation analyses.<sup>23,24)</sup> From the first-principles calculations within the local density approximation (LDA), Wills et al. have pointed out that there is a correlation between the shear modulus,  $C'=(C_{11}-C_{12})/2$  and the structural energy difference between bcc and fcc,  $\Delta E=E_{\text{bcc}}-E_{\text{fcc}}$  ( $E$  is the total energy), in cubic transition metals.<sup>23)</sup> For example, the shear modulus of  $C'$  in fcc increases as the  $\Delta E$  increases when the ground state is the fcc.<sup>23)</sup> This trend has also appeared in the computational results shown in Fig. 3 in the previous section. A similar consideration has been also made by Mehl et al. from the U.S. Naval Research Laboratory, in which they have pointed out that  $\Delta E$  is likely to correlate with the melting point based on the entanglement of the Born criterion described above.<sup>24)</sup>

The Bain deformation is the tetragonal strain deformation of cubic crystal as shown in Fig. 5(a) proposed by Bain in 1924 as a model of the martensitic transformation of steel.<sup>25)</sup> Under the small strain applicable to the elastic theory, the strain energy in cubic crystals is described as:<sup>26)</sup>

$$E_{\text{str}} = \frac{1}{2} C_{11}(e_{11}^2 + e_{22}^2 + e_{33}^2) + C_{12}(e_{11}e_{22} + e_{22}e_{33} + e_{33}e_{11}) + \frac{1}{2} C_{44}(e_{12}^2 + e_{23}^2 + e_{13}^2) \quad (1)$$

Therefore, if the distortion corresponding to Fig. 5(a),

$$e_{11} = e_{22} = \frac{e}{2\sqrt{3}}, e_{33} = -(e_{11} + e_{22}), \text{ other } e_{ij} = 0 \quad (2)$$

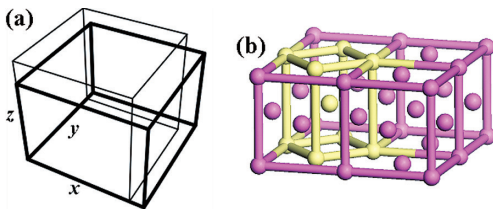


Fig. 5 Schematic illustrations of (a) Lattice deformation under Bain strain and (b) Body centered tetragonal (bct) crystal structure inside fcc one

is substituted in Eq. (1), the following simple relation is derived,

$$E_{\text{str}} = \frac{1}{2} C' e^2, \left( \because C' = \frac{C_{11} - C_{12}}{2} \right). \quad (3)$$

This expression describes that the curvature of the potential energy curve associated under the infinitesimal strain in the Bain path deformation directly leads to the shear modulus of  $C'$ . Figure 5(b) shows the atomistic model for the fcc crystal lattice. From a slightly different viewpoint, the fcc lattice is considered to be formed by the bct lattice indicated by white atoms. When the deformation in this lattice is provided as shown in Fig. 5(a), it can be imagined that the bct lattice inherent in a certain amount of distortion coincides with the bcc lattice. This is the reaction path for the martensitic transformation in steel originally imaged by Bain.<sup>25)</sup> Since some characteristic crystal orientation relationships with the parent phase (i.e. fcc phase) have been observed in the martensitic transformations of steels, the Bain path today does not necessarily represent the actual fcc-bcc phase transition path.<sup>27-29)</sup> However, due to the convenience of grasping energetic trends and to the theoretical usefulness for establishing concept, the Bain path is still an important concept that is used for various theoretical researches at present.<sup>21)</sup>

The theoretical concepts like the Bain path including physical quantities that can be experimentally constructed using the shear modulus  $C'$  have been currently extended. This is because these concepts can provide, in the situations of experimental and theoretical discussion, useful knowledge on the energy barriers and the rigidities existing around the ground state. One of them is the PALI strain proposed by Boyer. In the PALI strains, the change of primitive vectors through an orthorhombic strain acting on a fcc lattice can be expressed as a product of the following matrices,

$$\mathbf{a} = \begin{pmatrix} \mathbf{a}_1 \\ \mathbf{a}_2 \\ \mathbf{a}_3 \end{pmatrix} = \frac{1}{2} \begin{pmatrix} 0 & a & a \\ a & 0 & a \\ a & a & 0 \end{pmatrix} \begin{pmatrix} (1+b)^{-\frac{1}{3}} & 0 & 0 \\ 0 & (1+b)^{-\frac{1}{3}} & 0 \\ 0 & 0 & (1+b)^{\frac{2}{3}} \end{pmatrix} \begin{pmatrix} 1 & c & 0 \\ c & 1 & 0 \\ 0 & 0 & (1-c^2)^{-1} \end{pmatrix} \begin{pmatrix} \hat{x} \\ \hat{y} \\ \hat{z} \end{pmatrix}. \quad (4)$$

In Fig. 6, we show the schematic illustrations of lattice deformations under the PALI strain described by Eq. (4). In the PALI strain, similar to the Bain strain in Eq. (3), the following relationship with

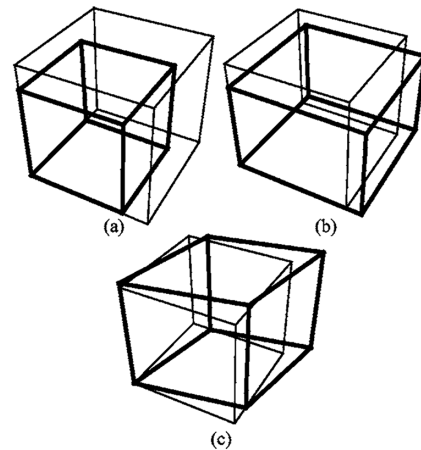


Fig. 6 Schematic illustrations of lattice deformations under the PALI strain defined by Eq. (4). (a) Change in the lattice constant  $a$  produces a stress proportional to the bulk modulus  $B_0$ , (b) Change in  $b$  produces a stress proportional to  $C_{11} - C_{12}$ , and (c) Change in  $c$  produces a stress proportional to  $C_{44}$ .

the observable elastic constants can be derived in the cubic systems under the infinitesimal strain limit.

$$\begin{aligned} B_0 &= \frac{C_{11} + 2C_{12}}{3} = V \frac{\partial^2 E}{\partial V^2}, \quad C' = \frac{C_{11} - C_{12}}{2} \\ &= \frac{3}{4V} \frac{\partial^2 E}{\partial b^2}, \quad C_{44} = \frac{1}{4V} \frac{\partial^2 E}{\partial c^2} \end{aligned} \quad (5)$$

**Figure 7** shows an example of the contour plot of energy ( $E$ ) under the PALI strain. The PALI strain found by Boyer<sup>30)</sup> is often called the magic strain.<sup>31)</sup> Since the fcc crystal lattice can be transformed into itself by the physically allowed (symmetric) shear-strain tensors indicated by Eq. (4), three types of selections are present for the strain parameters  $b$  and  $c$  as the fcc structure ( $\circ$  points) on the contour plot shown in Fig. 7(a). Van de Waal has subsequently shown that the PALI strains, which describe the lattice self-transformation including the information on the elastic constants observable under the infinitesimal strain limit, can be derived for any lattice.<sup>32)</sup>

The cross-section curve along  $c=0$  in Fig. 7(b) is the Bain path energy curve (the so-called classical meaning), in which the points at  $b=0$  and  $b=1/\sqrt{2}-1$  correspond to the fcc and the bcc lattices, respectively. When the fcc (bcc) lattice is in the ground state, the energy curve of the Bain path shows the maximum value in the bcc (fcc) lattice. Since the curvature in the vicinity of the ground state (fcc lattice:  $b=0$  in Fig. 7(b)) gives strictly the shear modulus of  $C'$  in the corresponding lattice, where the maximum value at the conflicting lattice (i.e. bcc lattice:  $b=1/\sqrt{2}-1$ ) is likely to increase as this curvature becomes larger in the energy curve of the Bain path, the indication by Wills et al. described above<sup>23)</sup> is assumed to be very plausible.

Moreover, the energy curve near the bcc lattice along the Bain path is upwardly convex. The reason why the shear modulus of  $C'$  has a negative value (Fig. 3(b)) and the elastic instability (Born instability) appears can, therefore, be geometrically understood from the energy curve along the Bain path. This suggests that the relative crystal stability between bcc-fcc essentially comes from the elastic instability of the associated conflicting lattice. Grimvall et al.<sup>21)</sup> have reviewed that the relationship between the phase stability and the elastic instability among the conflicting lattices described in this section is the correlation having universality established in many bcc-fcc (more generally the close-packed lattice) metallic systems.

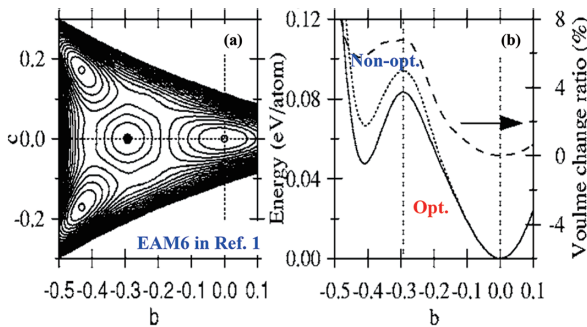


**Fig. 7** Contour plots of the total energy in the PALI strain (left panels) and energy plots along the  $c=0$  line (right panels) computed by allowing for volume relaxation for EAM6 in Ref. 1). The contours are shown in every 0.01 eV/atom. In right panels, we also show the volume change under distortion by the dashed line. The energy plots via non-optimization of volume are also depicted by the dotted line. Energy is measured from the total energy of the equilibrium fcc structure based on the corresponding potential. The saddle point  $\bullet$  corresponds to the bcc structure, while the fcc structure is located at the open circle points  $\circ$ .

### 2.3 Phase transition temperature and lattice dynamical instability

If crystalline solids are greatly distorted like Bain deformation, the lattice dynamical instability such as the phonon instability and/or the elastic instability in different modes, which cannot be expected in advance from the corresponding strain energy curves, is sometimes induced in the crystals.<sup>1)</sup> **Figure 8** shows an example of the lattice dynamical instability under the Bain deformation in the fcc-Al system,<sup>1)</sup> which has been calculated using the EAM model submitted by Mishin et al.<sup>33)</sup>

As shown in Fig. 8(b), when the system is exposed to a certain degree of external strain along the Bain path, the soft mode in which the phonon frequency decreases at the  $[1/2 \ 1/2 \ 1/2]$  point in the Brillouin zone can be observed in the crystal concerned. If the system undergoes even larger distortion, the phonon instability, in which the corresponding frequency becomes a complex number, is first induced at a location far from the zone center of the  $\Gamma$  point as shown in Fig. 8(c). When the strain parameter of  $b$  further increases, the frequency becomes a complex number even in the vicinity of the Brillouin zone center (i.e.  $\Gamma$  point) as shown in Fig. 8(d), which physically indicates that the long-term elastic instability is apparent in the crystals. In other words, the crystal lattice cannot withstand such very large strain along the Bain path, and the spontaneous deformation in the system is generally induced by the lattice dynamical instability described above.

In **Fig. 9**(a), we show the location of instabilities in the energy curve along the Bain path calculated for some EAM-Al models. The open ( $\circ$ ) and closed circles ( $\bullet$ ) indicate the phonon and elastic instabilities, respectively. In addition, the relations between the thermodynamic melting temperatures and the energy locations of instabilities are depicted in Fig. 9(b). A strong linear correlation between the thermodynamic melting temperatures and the energy locations of phonon instabilities has been found as shown in Fig. 9(b).<sup>1)</sup> The re-

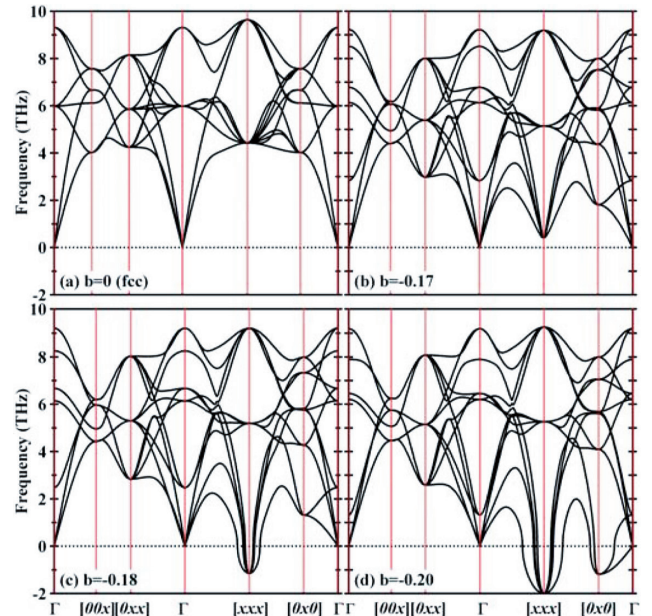


**Fig. 8** Phonon dispersion curves<sup>1)</sup> as a function of strain parameter,  $b$ , along the Bain path (see also Fig. 7) for an EAM-Al model<sup>33)</sup> These calculations are carried out using the conventional cell of the face-centered tetragonal (fct) structure. The negative values are used to plot imaginary frequencies for convenience.  $x$  denotes the value of 1/2 in units of reciprocal unit vectors.

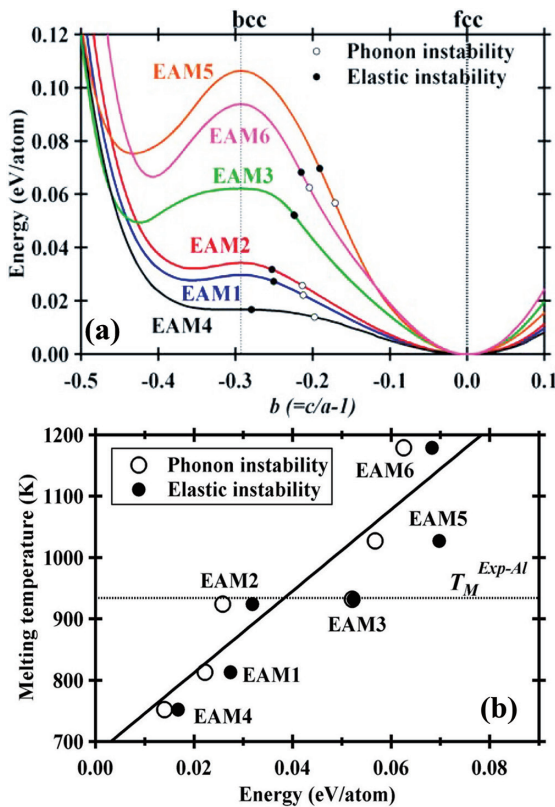


Fig. 9 (a) Typical examples of energy curves along the Bain path calculated using some EAM models of Al<sup>1)</sup> We also show the location of instabilities for each potential model in the energy curve along the Bain path. (b) Relation between the thermodynamic melting temperatures and the energy locations of phonon (○) and/or elastic instabilities (●) in (a)

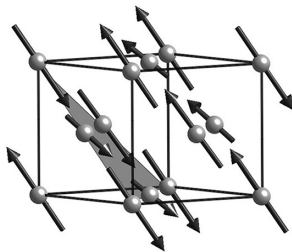


Fig. 10 Schematic of the phonon instabilities first appeared under strain along the Bain path<sup>1)</sup> The unstable mode corresponds to the displacements in approximately the  $\langle 112 \rangle \{111\}$  directions.

result suggests that the melting behavior of crystals is essentially related to not only the energetics, but also the lattice dynamic instabilities. As shown in Fig. 8(c), we have described that the unstable phonon mode that first appeared along the Bain path strain is located at the  $[1/2 \ 1/2 \ 1/2]$  point in the Brillouin zone. From the analyses of the eigenvectors of the dynamical matrix, the unstable mode is also found to correspond to the displacements in approximately the  $\langle 112 \rangle \{111\}$  direction for all of the adopted EAM models, among which the crystallographic geometry of the instability is exemplified in Fig. 10.

These facts indicate that the phonon instabilities that first appeared along the Bain path strain correspond to the  $\langle 112 \rangle \{111\}$  direction in the fcc lattice. It is more interesting to note that the vari-

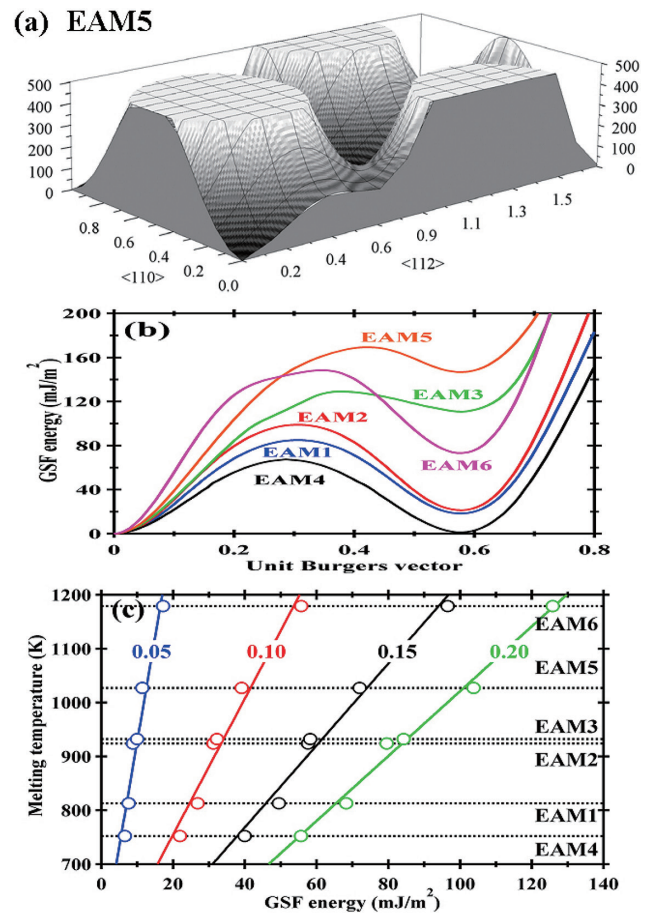


Fig. 11 (a) Example of  $\gamma$  surface for displacements along a  $(111)$  plane in fcc-Al with the equilibrium lattice constant ( $a_0$ ) The energy and displacement units are in  $\text{mJ}/\text{m}^2$  and in the unit Burgers vector,  $|b|=|a_0[101]/2|$ , respectively. The energy surfaces exceeding the value of  $500 \text{ mJ}/\text{m}^2$  are truncated. The corners of the plane and its center correspond to identical equilibrium configurations, i.e., the ideal fcc lattice. (b) Projections of the  $\gamma$  surfaces on the  $\langle 112 \rangle$  direction calculated using some EAM-Al potentials (c) Relation between the thermodynamic melting temperatures and the GSF (Generalized Stacking Fault) energies along the  $\langle 112 \rangle$  direction, where the internal figures of 0.05, 0.10, 0.15, and 0.20 show the displacement values expressed by the unit Burgers vector All these figures are reproduced from the original data in Ref. 1).

ants of the  $\langle 112 \rangle \{111\}$  direction correspond to the directions of the Heidenreich-Shockley partial dislocations and/or the twin directions in the fcc lattice. In other words, the atoms in the fcc lattice can spontaneously be displaced to this orientation without any energetic barriers under a certain strain along the Bain path. This suggests that the melting phenomenon in crystalline solids is related to the phenomena of the dislocation emissions and/or its kinetics in the associated solids.

To discuss this quantitatively, the computational result on the correlation between the generalized stacking fault energy surface (GSFE surface or  $\gamma$  surface) and the melting point<sup>1)</sup> is described in the final part of this section. The GSFE surface is the excess energy per unit area for a given relative displacement vector of one half of the crystal with respect to the other half when a perfect crystal is cut across the slip plane into two parts (Fig. 11 (a)). The basic concept

of the GSFE surface was first introduced by Vitek.<sup>34)</sup> Figure 11 (b) shows the projections of the (111) GSF energy surfaces on the  $\langle 112 \rangle$  direction calculated using the Al-based EAM potentials adopted in Ref. 1). The first energy maximum value in this curve is sometimes called the “unstable stacking fault energy”, and Rice has pointed out that it is an important material property serving as a resistance index of dislocation generation in the crystal.<sup>35)</sup> The next energy minimum is the “stable stacking fault energy”.

In the initial slip displacement region along the  $\langle 112 \rangle$  direction around the ideal fcc configuration, we have found that there is clearly a strong linear correlation between the melting temperatures and the GSF energies as shown in Fig. 11 (c).<sup>1)</sup> For the solid-liquid phase transition phenomena, the concept of the “dislocation-mediated melting” whereby the generation of dislocation in the crystal is an important ingredient for solid melting phenomena has been in existence for some time.<sup>36–38)</sup> Our computational result described in this chapter<sup>1)</sup> suggests again that the melting phenomenon is a dislocation-induced type first-order phase transition<sup>36–38)</sup> when the transition is viewed from the initial state side of the solid phases.

### 3. Bain Path Energetics and Martensitic Transformation in Iron

In the previous chapter, based on the energetics for the Bain strain and/or the PALI strain, the presence of an elastic conflicting lattice such as bcc-fcc, and the relationship between the thermodynamic stability and lattice dynamical instability have been described. In iron-based alloys such as steels, the phase transitions among the conflicting lattices such as martensitic transformations (fcc  $\longleftrightarrow$  bct) and/or  $\gamma \longleftrightarrow \alpha$  transformations (fcc  $\longleftrightarrow$  bcc) actually exist. This chapter describes from the framework of the band model of ferromagnetism (Stoner model) how the Bain path energy of iron (Fe) is changed by the presence of magnetism (or spin polarization),<sup>2)</sup> and introduces our relevant experimental studies on steel-based martensitic transformation.<sup>14–17)</sup>

#### 3.1 Bain path energetics in iron viewed from band model of ferromagnetism: Effect of magnetism

Iron and/or iron-based alloys are the structural materials with the longest history having important positions in commercial activities. From the viewpoint of microscopic materials science, they are also the systems with many unexplained parts regarding both the phase stability and the lattice dynamical stability. This stems mainly from the complex spin structures in the solid phases with the Fe element. The physical interpretation on the phase stability near the fcc lattice is particularly difficult. Various spin states for the Fe-based alloys with fcc structure, such as non-magnetic (NM), ferromagnetic (FM), antiferromagnetic (AF), spin spiral (SS), and non-collinear (NC), are degenerated with an energy difference of only several mRy/atom (1 Ry = 13.6 eV) depending on the associated atomic volume.<sup>39)</sup>

However, the lattice-mechanical reciprocity (or elastic conflicting) among bcc-fcc (see Sec. 2.2) in the ferromagnetic (FM) and nonmagnetic state (NM) has been confirmed from the analyses on the phonon dispersion curves within the framework of the Density Functional Theory (DFT).<sup>40, 41)</sup> Hsueh et al. have performed the fixed-spin-moment calculations for bcc-Fe, and reported that the lattice dynamical stability is available in the FM state with a magnetic moment of about  $\mu = 2.2$  and that the elastic instability with the complex frequency near  $\Gamma$  point appears near the NM state.<sup>40)</sup> In contrast, Zhang has indicated from a similar theoretical analysis that the lattice dynamic stability for fcc-Fe is available near the NM state conflicting with the bcc lattice and that the elastic instability with the complex frequency near  $\Gamma$  point appears in the FM state with about  $\mu = 2.0$ .<sup>41)</sup>

The lattice dynamic instabilities<sup>40, 41)</sup> indicated by them can be visually understood by obtaining an energy map on the Bain deformation for the Fe system based on the fixed magnetic moment calculations. Our computational result is shown in Fig. 12. Figure 12 (a) shows the energy curve surface of the Bain deformation (in eV/atom unit: the energy for NM-fccFe ( $\circ$ ) is used for the energy standard) when the magnetic moment is changed from the non-magnetic state

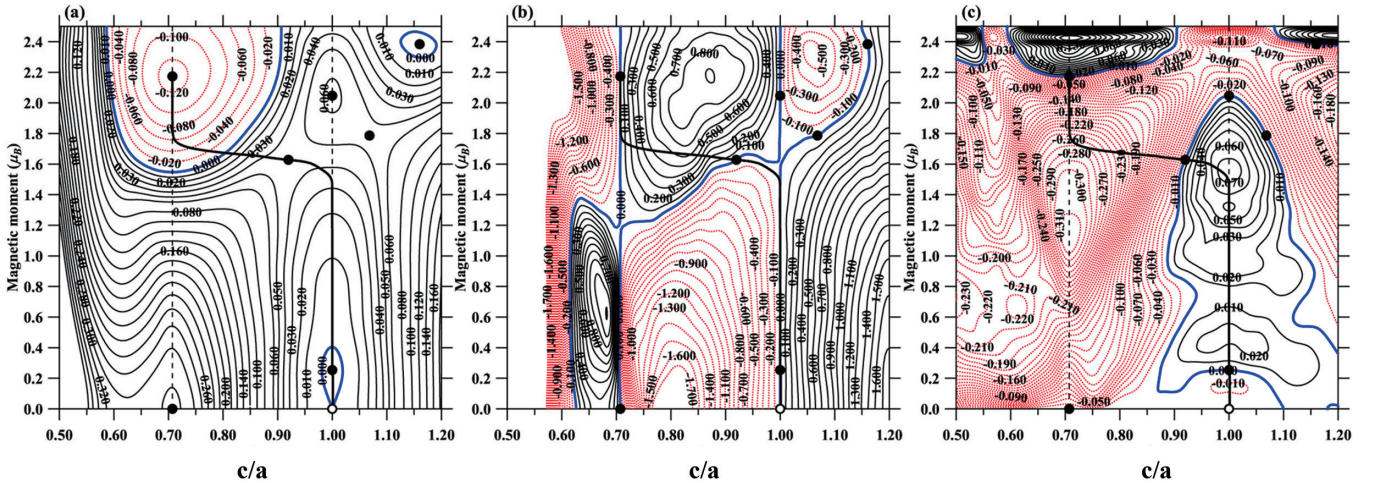


Fig. 12 Two dimensional contour plots of (a) Total energy surface  $E(\mu, c/a)$  (in eV/atom), the energetic field surfaces for (b)  $(\partial E / \partial (c/a))_\mu$ , and (c)  $(\partial E / \partial \mu)_{c/a}$  as a function of magnetic moment ( $\mu$ ) and Bain-path shear parameter ( $c/a$ ) along with the atomic volume optimization. The energy contour lines in (a) are labeled relative to the total energy for NM-fcc with the GGA equilibrium atomic volume ( $V_{EO}^{NM-fcc} = 10.15 \text{ \AA}^3/\text{atom}$ ). The zero line in each contour is drawn by the thick blue line. The red dotted lines and the black solid ones indicate the negative and positive values, respectively. The black circles show the configurations becoming the local minimum and/or the saddle points in the energy map of (a), which satisfy the condition of  $(\partial E / \partial (c/a))_\mu = (\partial E / \partial \mu)_{c/a} = 0$ . The thick solid line depicted in each contour is the hypothetical reaction coordinate (RC), which has been numerically searched by the steepest-descent method from the saddle point of  $(\mu, c/a) = (1.63, 0.92)$ . For reference, the bcc and fcc configurations are shown by the vertical broken lines ( $c/a = 1/\sqrt{2}$  and 1) and the location of NM-fcc is denoted by the open circle.

( $\mu=0$ ) to the ferromagnetic state ( $\mu=2.5$ ). Since the magnetovolume effect has a large effect on the binding properties in a ferromagnetic state, these analyses were carried out using the computational technique that allows the atomic volume relaxation with the fixed values of the Bain path variable ( $c/a$ ). The maps shown in Fig. 12 were deduced by the  $50 \times 50$  points calculations. The GGA (generalized gradient approximation) is also adopted for the electron many-body correlations. In Fig. 12, the vertical broken lines at  $c/a=1/\sqrt{2}$  and  $c/a=1$  correspond to the bcc and the fcc structures, respectively. Figure 12(b) and (c) are the differential field maps of total energy  $E$  for the Bain deformation variable ( $c/a$ ) and magnetic moment ( $\mu$ ), respectively ((b)  $(\partial E/\partial(c/a))_{\mu}$ , (c)  $(\partial E/\partial\mu)_{c/a}$ ). For each contour plot, the red line indicates the negative value, the black line indicates the positive value and the thick blue line indicates the zero value. In addition, the solid circle ( $\bullet$ ) in the figure satisfies the conditions of  $(\partial E/\partial(c/a))_{\mu}=(\partial E/\partial\mu)_{c/a}=0$ , which imply that those points correspond to the energy local minimum values and/or local maximum values (or saddle points). The ground state within the present computational scheme adopted becomes the ferromagnetic bcc of ( $\mu, c/a$ ) = (2.2,  $1/\sqrt{2}$ ) indicated by the solid circle ( $\bullet$ ) at the upper left of Fig. 12(a).<sup>42)</sup>

Focusing on Fig. 12(b), the zones of the magnetic moments with the elastic instability can be clearly identified both for bcc and fcc lattices. In bcc ( $c/a=1/\sqrt{2}$ ), the elastic instability ( $C'$  instability: Refer to Sec. 2.2.) appears in the zone with a low spin region of  $\mu < 1.2$ . This indicates that the Bain path energy curve gives the upward convex at the associated point as shown in the right panel of Fig. 7. In contrast, in fcc ( $c/a=1$ ), the elastic instability appears in the zone with a high spin region of  $\mu > 1.6$ . These results completely support the lattice dynamical instability analyses from the phonon dispersion curves described above.<sup>40, 41)</sup> From our preliminary calculations, the high spin side might also have the threshold of elastic instability. The elastic instability is found to appear in the zone of ( $\mu < 1.2, \mu > 4.0$ ) for bcc and of ( $1.6 < \mu < 3.5$ ) for fcc, respectively.

The zone of  $1.2 < \mu < 1.6$  for the magnetic moment is physically interesting. Both bcc and fcc have the minimum value with shallow energy (Both phases have the lattice dynamical stability. Refer to Fig. 13(a):  $\mu=1.4$ ), where the energy barrier between both lattices

almost diminishes. Such a zone is also used as the basic concept for developing the GUMMETALS,<sup>43, 44)</sup> whereas it may be difficult to achieve the property in the case of ferrous systems because the spin polarization must be controlled. The GUMMETALS with Titanium-based alloy compositions are the materials that show unique deformation modes where the plastic deformations are not caused by the dislocation motions.<sup>43, 44)</sup> It is interesting to note that those materials have been searched near the compositional boundary transiting from hcp to bcc in Ti alloy systems where the elastic conflicting between the bcc and the close-packed structures can be collapsed.<sup>43, 44)</sup>

The thick black lines displayed on each map in Fig. 12 are the hypothetical reaction coordinate (RC: reaction coordinate) between the associated fcc-bcc transitions, where the hypothetical RC through the saddle point of  $\varphi \equiv (\mu, c/a) = (1.63, 0.92)$  has been determined by the steepest descent method using the gradient  $\nabla\varphi$ . The meaning of ‘‘hypothetical’’ is that the actual reaction system might not pass this coordinate because the physical relaxation rates of the magnetic moment ( $\mu$ ) and the Bain path variable ( $c/a$ ) are possibly different. Figure 13(a) shows some projection curves on the line of  $\mu = \text{const.}$  in Fig. 12(a).

For reference, the RC obtained from the steps above is also shown. The RC energy barrier of fcc  $\rightarrow$  bcc obtained within the framework of this analysis is about 50 meV/atom and the value of bcc  $\rightarrow$  fcc is about 180 meV/atom. As shown in Fig. 13(a), the fcc lattice becomes energetically unstable and the energetic stability for the bcc lattice becomes apparent as the magnetic moment increases. In addition, in the regions where the magnetic moment is small, the elastic instability (Born instability) appears in which the energy curve in the vicinity of the bcc lattice is upwardly convex. Conversely, the elastic instability is found to appear in the vicinity of the fcc lattice where the magnetic moment becomes large. Thus, in iron and/or iron-based alloys, the magnetic interaction plays an essential role with regard to the thermodynamic stability and the elastic instability between bcc-fcc lattices.

Figures 13(b) and (c) shows the behavior of the magnetovolume effect as a function of the magnetic moment ( $\mu$ ).  $\omega_{\text{NM-fcc}}$  represents the coefficient of volume expansion based on the atomic volume in non-magnetic fcc. The magnetovolume effect refers to a phenome-

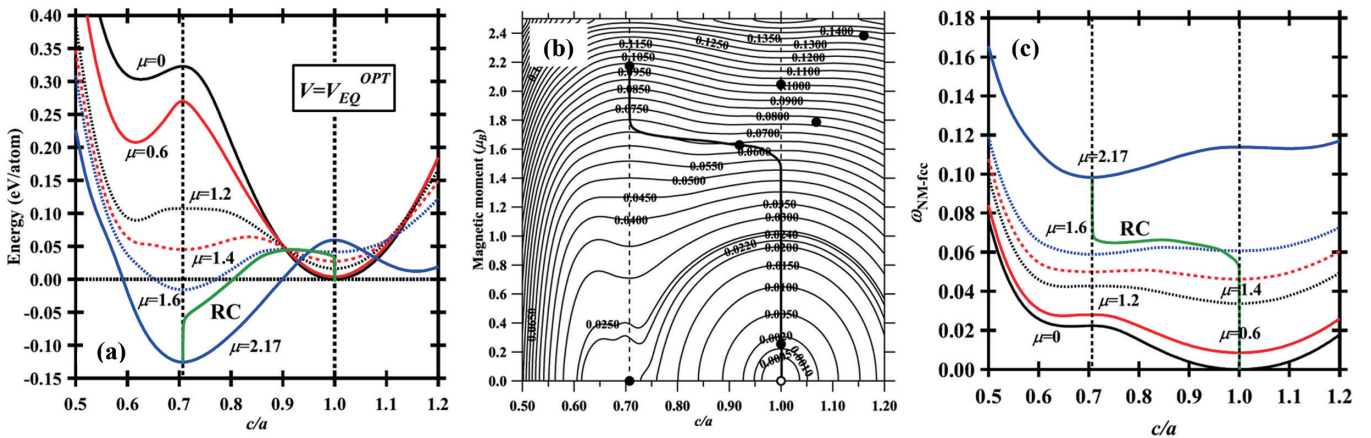


Fig. 13 (a) Calculated total energies as function of  $c/a$  for the systems with the optimized atomic volume projected on the lines of  $\mu = \text{const.}$  in Fig. 12(a). Energy is measured from the total energy for the equilibrium NM-bcc with  $V = V_{EQ}^{\text{NM-fcc}}$ . (b) Optimized volume surface ( $\omega_{\text{NM-fcc}}(\mu, c/a)$ ) as a function of magnetic moment ( $\mu$ ) and Bain-path shear parameter ( $c/a$ ). The atomic volume is plotted by the increment ratio based on the volume for the equilibrium NM-fcc state. (c) Atomic volume curves as a function of  $c/a$  projected on the lines of  $\mu = \text{const.}$  in (b). The thick green lines depicted in (a) and (c) are the hypothetical reaction coordinates (RC).

non in which the magnetic properties of materials and their volumes change by mutually interacting with each other. Figure 13(c) shows that we can observe the atomic volume expansion of about 10% with the transition from non-magnetic fcc to ferromagnetic bcc in the case of iron. In the present theoretical framework where the Stoner model's so-called band theory of ferromagnetism<sup>45)</sup> is considered, we can obtain the physical picture on the fcc→bcc transition for iron, in which the local ferro-magnetization due to the change of the magnetic moment promotes the lattice dynamical instability for fcc and the ferromagnetic bcc with the dynamical stability is induced.

One of the merits for using the Stoner model is that it becomes possible to consider the factor of the lattice dynamical instability during the Bain path strain as a response phenomenon of the electronic structure due to the distortion perturbation. **Figure 14** shows an example of the electronic structural responses around the Fermi level, when a small Bain strain perturbation is added for the bcc lattice ((a)  $\mu=1.00$ : Unstable, (b)  $\mu=1.40$ : Stable) and the fcc lattice ((c)

$\mu=1.40$ : Stable, (d)  $\mu=1.85$ : Unstable) with the dynamical stability and instability induced by the associated magnetic moments. The black and color lines in Fig. 14 show the electronic band dispersions unperturbed and perturbed by the small Bain strain, respectively. We have found, as shown in Figs. 14(a) and 14(d), that the lattice dynamical instability becomes apparent in the systems where the shape of the Fermi surface greatly changes with respect to the distortion perturbation. In contrast, as shown in Fig. 14(b) and (c), the lattice dynamical stability has appeared in the systems where the Fermi surface shape is not sensitive to the associated strain perturbation.

In the final part of this section, we briefly mention the lattice dynamical stability observed for the  $\delta$ -bcc phase at high temperature in pure iron. The  $\delta$ -bcc actually exists as a thermodynamically stable phase at high temperature exceeding the Curie point while the bcc with nonmagnetic state ( $\mu=0$ ) has the elastic instability as described above. The readers may, therefore, question whether the  $\delta$ -bcc can be dealt with as the band nonmagnetic phase. There is a specific fluctuation of magnetic spins (the specific spin configuration) as an important degree of freedom that exceeds the description limit of

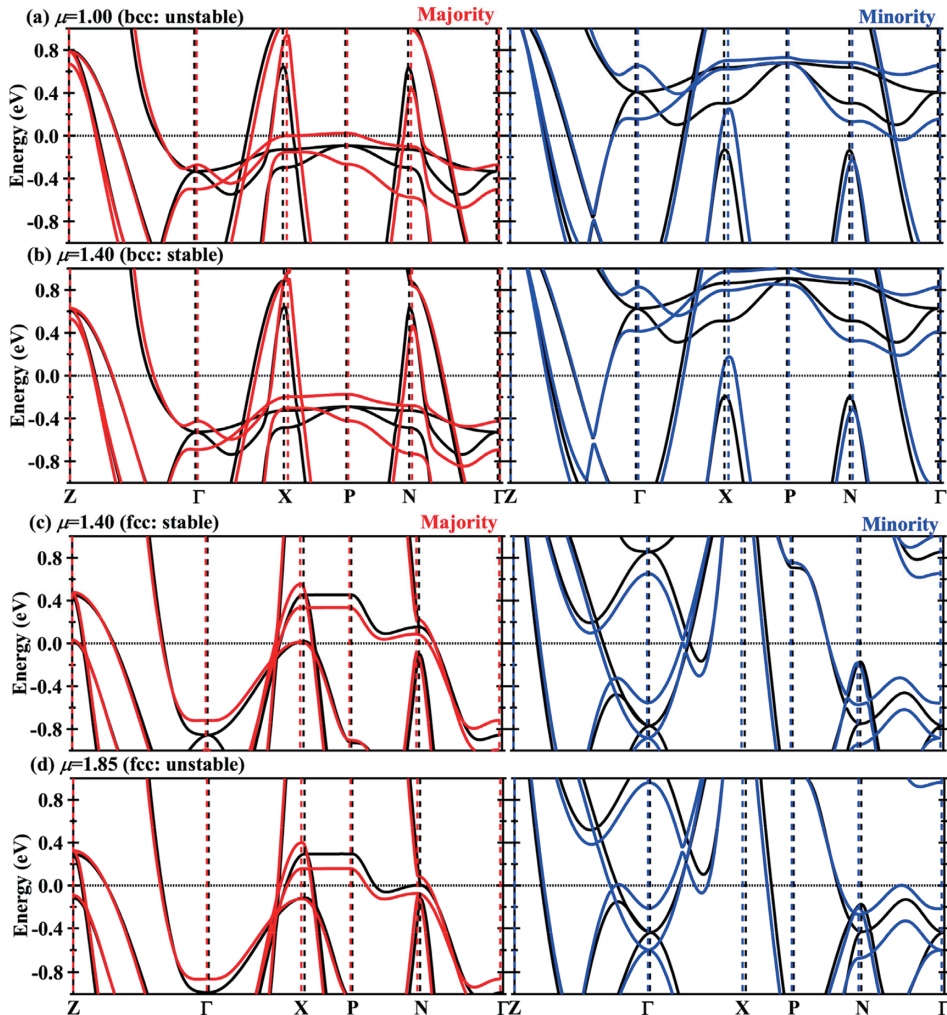


**Fig. 14** Electronic band structure response around the Fermi level perturbed by the small Bain-path distortion. We show the responses for (a)  $\mu=1.00$  in bcc with the lattice-dynamical instability, (b)  $\mu=1.40$  in bcc with the stability, (c)  $\mu=1.40$  in fcc with the stability, and (d)  $\mu=1.85$  in fcc with the instability. The left and right panels show the band dispersions in majority and minority spin states, respectively. The black and color lines depicted in each panel indicate the electronic structure unperturbed and perturbed by the small Bain-path distortion, respectively.

the Stoner model described in this manuscript. Several methods for approximating the spin specific fluctuations have recently been developed to describe the paramagnetic states. Based on these methods, it has been reported that the elastic instability may not appear in the Bain path energy curve in the paramagnetic bcc.<sup>46)</sup> It has also been confirmed that the phonon instability does not appear in the phonon dispersion in the paramagnetic bcc at finite temperature (T=900°C).<sup>47)</sup>

**3.2 In-situ measurement of elastic properties during martensite transformation based on the concept of Bain path energetics**

Regarding the dependence of the element compositions on the phase transformation temperature for steels, various research expressions have been submitted over a long period of time. For example, the following formula relating to the starting temperature of martensite transformation is well known.<sup>48)</sup>

$$M_s(K, \text{at}\%) = 818 - 71C + A1 + 7Co - 14Cr - 15Cu - 23Mn - 8Mo - 6Nb - 13Ni - 4Si + 3Ti - 4V + 0W \quad (6)$$

The above formula describes a thermodynamic index indicating the phase stability for the austenite phase (the fcc phase) at the low temperature side. The physical meaning and the mechanism at the atomistic level on the weighting factor and/or the ± symbol of the element for the transformation temperature are not yet understood. As described in the previous section, it will be qualitatively expected in iron-based alloys that the lattice dynamical instability for the bcc state disappears due to the magnetic interaction accompanying the decrease of temperature, and that the fcc state having the dynamical stability at high temperature can transform to the bcc state at a certain temperature. However, from the viewpoint of such lattice energetics and/or dynamics, there have been few attempts to conduct experimental studies on the martensitic transformation processes in steels.

Figure 15 shows the effect of impurities ((a) Carbon,<sup>17)</sup> (b) Aluminum) for the Bain path energy curves in the non-magnetic Fe (NM-Fe) (for the calculation method, refer to Ref. 17)). As the carbon concentration increases, the energetic instability for bcc monotonically increases as shown in Fig. 15(a). In contrast, as shown in Fig. 15(b) for aluminum, the energetic instability for bcc is found to decrease monotonically with the increase in the concentration. The total energy difference between bcc and fcc ( $\Delta E \equiv E_{NM-bcc} - E_{NM-fcc}$ ) as

a function of the impurity concentration is shown in Fig. 15(c). The carbon element enhances the relative stability of the fcc structure with respect to the bcc and conversely aluminum is an element that decreases the relative stability of fcc. Furthermore, this effect is found to have a strongly linear correlation with each concentration. Therefore, the weighting factors and the physical meaning of ± symbols in Eq.(5) that show that the phase stability of the austenite phase (fcc phase) at the low temperature side can be qualitatively reproduced for carbon and aluminum based on the present energetic considerations.

As described in Sec.2.2, the energy curve of the Bain path deformation quantitatively includes the information of shear modulus. Therefore, if the element dependence on the shear modulus in the fcc lattice during the transformation process can be measured *in-situ*,<sup>14)</sup> it may be possible that a part of the energy curve in question before transformation, which gives the phase stability index of the austenite phase (γ phase), is grasped. Thus, focusing on the carbon element that remarkably increases the relative stability of fcc, we performed direct *in-situ* measurements of the elastic modulus during the martensitic transformation for the steels in which the amount of carbon has been changed, using the ultrasonic pulse sing-around method.<sup>15-17)</sup>

Details of experiments are covered by our original references<sup>15-17)</sup> and the overview thereof is shown in Fig. 16. As described in the upper part of Fig. 16, 9Ni steels in five levels that changed the carbon content were prepared in this experiment. After being austenitized at 850°C, the elastic modulus was measured in the cooling process from 2°C/s to 200°C and 1°C/s to 140°C. The phase transformation temperature (M<sub>s</sub> point or B<sub>s</sub> point) was determined by dilatometric measurements. It is metallographically confirmed that T1 and T2 are bainite and T3–T5 are martensite.<sup>49)</sup>

Figure 16(a) shows the change of shear modulus from 400°C to the phase transformation temperature for T1, T3, and T5 specimens. The lattice dynamical instability and/or its precursory behavior (i.e. soft mode and softening of stiffness), which are often observed in the martensitic transformation for the shape memory alloy systems,<sup>50, 51)</sup> have not been observed in the present *in-situ* measurements, and the shear modulus is found to simply increase with the decrease in temperature. The temperature dependency of shear modulus near the phase transformation temperature (near the M<sub>s</sub>

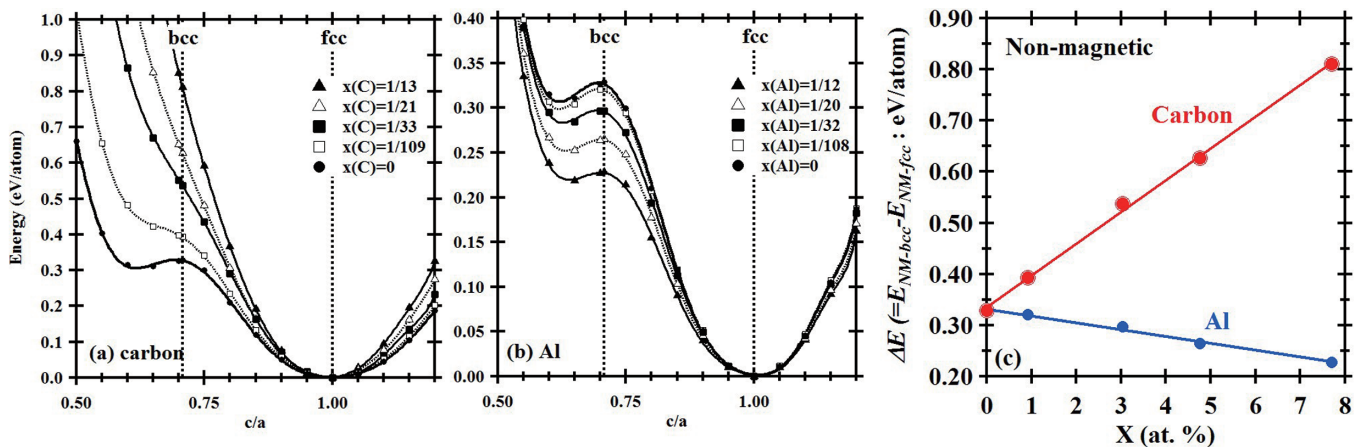


Fig. 15 Impurity effects of (a) carbon<sup>17)</sup> and (b) aluminum on the Bain-path energy curves in non-magnetic Fe (NM-Fe), (c) Structural energy difference between NM-bcc and NM-fcc ( $\Delta E \equiv E_{NM-bcc} - E_{NM-fcc}$ ) as a function of impurity contents. The energetic stability of fcc is monotonously increased and decreased with the contents of carbon and aluminum, respectively, which qualitatively agree with the physical meaning for the plus-minus sign of the coefficients of C and Al in Eq.(6).

Specimen	C (Mass Percent)	Si (Mass Percent)	Mn (Mass Percent)	Ni (Mass Percent)	Fe
T1	0.016	0.25	1.0	9.03	bal.
T2	0.1	0.27	1.0	9.28	bal.
T3	0.2	0.25	1.0	8.98	bal.
T4	0.31	0.26	1.0	9.25	bal.
T5	0.45	0.25	1.0	9.03	bal.

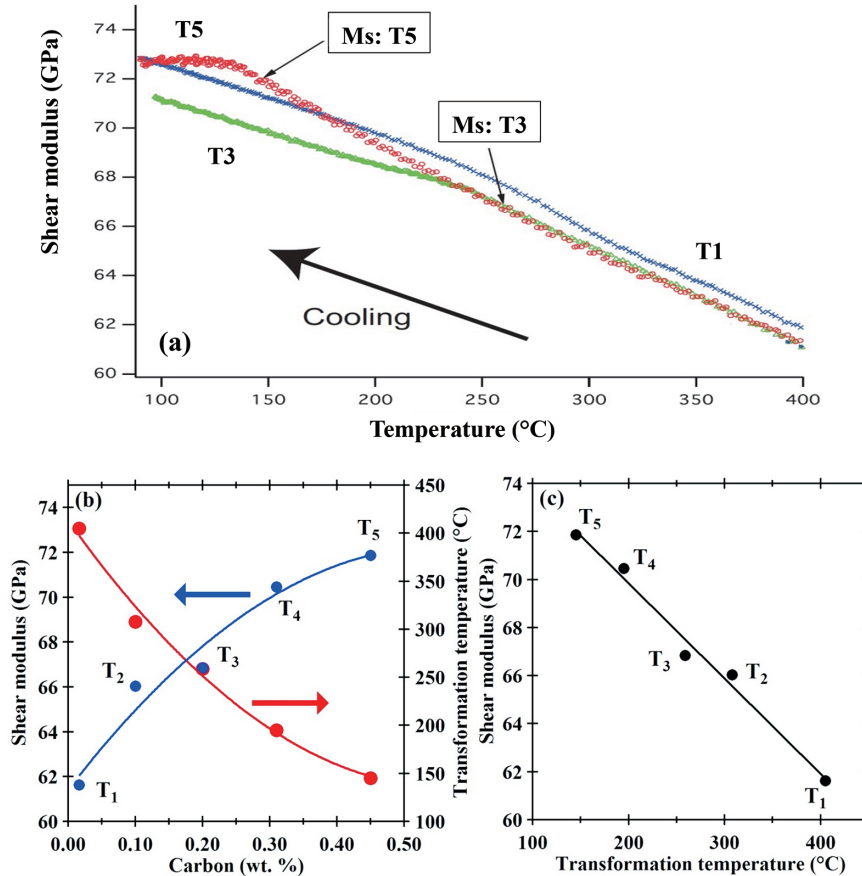


Fig. 16 Top panel shows the chemical composition for each specimen analyzed in the experiments<sup>15-17</sup>  
 (a) Shear modulus measured in T1, T3, and T5 steels in the course of cooling cycle<sup>15,16</sup>  
 The arrows indicate the locations of transformation temperature measured by dilatation method for T3 and T5.  
 (b) Shear modulus at the (Martensitic:  $M_s$  and/or Bainitic:  $B_s$ ) transformation temperature (left) and the corresponding transformation temperature (right) as a function of carbon contents<sup>15-17</sup>  
 (c) Shear modulus at the  $M_s$  and/or  $B_s$  temperature as a function of corresponding transformation temperature<sup>15-17</sup>

point or  $B_s$  point) has been changed from the extrapolation line at the high temperature side to the higher shear modulus side (i.e. the excess shear modulus),<sup>15-17</sup> and the behavior preventing the lattice dynamical instability of austenite (fcc) due to lowering temperature has been observed.

We show the transformation temperature and the shear modulus at the transformation temperature with respect to the carbon concentration in Fig. 16(b). It has been found that there is a clear inverse correlation between both. This is the experimental verification of the concept of Bain path energetics (Fig. 16(a)) that the shear modulus is correlated with the associated phase stability. Figure 16(c) shows the relationship between the transformation temperature and the shear modulus in the system studied. A strong linear correlation among them has been observed in the present study. These results indicate that the curvature change of the Bain deformation energy

curve with the carbon atom is an important elementary process for stability of the austenite phase at the low temperature side. Our recent research also suggests that this change in the shear modulus due to carbon elements affects the relaxation process in the martensitic transformation process and that the change in the shear modulus is experimentally confirmed to affect the crystallographic variant selection of the martensite structures.<sup>49</sup>

#### 4. Conclusions

In this article, we have outlined how the elastic dynamical properties in crystalline solids are related to the physical properties on the thermodynamic phase stability based on our theoretical studies from the microscopic perspective. In addition, as an experimental study related to these theoretical studies, the research on *in-situ* measurements of elastic properties during the martensitic transfor-

mation in steels has been introduced. The phase transformation phenomena in crystalline solids are assumed to be often related to the lattice dynamical instability whereby the associated solids become dynamically unstable and cannot retain their structures. Since the electronic structure in steels is so complex, researches on steels from the materials scientific perspective as described in this report have only just begun. The usefulness of artificial intelligence (AI) and machine learning (ML) has been recognized also for materials science and technology. The aim of AI and ML is basically to extract the essential principles from a large amount of data. This hot activity is in fact equivalent to the activities in natural science to date itself.

The research described in this paper is rather an approach with the strong aspect of classical human data mining based on condensed matter physics. While both approaches will play a complementary role for the time being, computational materials science based on the energetics that can reasonably connect phenomena and physics with different concepts is also a very exciting research field. In order to maximize the possibilities of steel materials, it is always important to scientifically understand the materials in question at any time. We conclude this paper with the wish that computational materials science proven by the mutual complement of humans and computers will contribute to this field together with the knowledge from advanced experimental studies.

#### Acknowledgments

This technical paper includes the joint research results by Dr. Masaaki Igarashi, Nippon Steel & Sumikin Chemical Co., Ltd., Dr. Hideki Yamagishi, Toyama Industrial Technology Center and Dr. Yuichi Komizo, emeritus professor of Osaka University and we are greatly indebted to the persons concerned.

#### References

- Moriguchi, K., Igarashi, M.: Correlation between Lattice-strain Energetics and Melting Properties: Molecular Dynamics and Lattice Dynamics Using EAM Models of Al. *Phys. Rev. B*. 74, 024111 (2006)
- Moriguchi, K., Igarashi, M.: Correlation Between Phase Transition Properties and Lattice-strain Energetics in Metallic Materials. *Journal of Smart Processing*. 2 (3), 102 (2013) (in Japanese)
- Raabe, D.: *Computational Materials Science*. Weinheim, Wiley-VCH, 1998
- Provatas, N., Elder, K.: *Phase-Field Methods in Materials Science and Engineering*. Berlin, Wiley-VCH, 2010
- Osuki, T., Moriguchi, K., Ogawa, K.: Prediction Solidification Microstructure of Austenitic Stainless Steel Using Multi-Phase Field Model. Preprints of the National Meeting of JWS. 2009s, 316 (2009) (in Japanese)
- Osuki, T., Moriguchi, K., Seki, A., Hirata, H., Ogawa, K.: Solution of Mechanism to Prevent Solidification Crack in Fully Austenitic Weld Metal Containing High Phosphorus with Crystallization of Cr Based Carbide Using Phase Field Method. Preprints of the National Meeting of JWS. 2012s, 114 (2012) (in Japanese)
- Kaido, H., Moriguchi, K.: Simulation Studies on Cottrell Locking Using Phase-field Method. Proceedings Book of the 3rd International Symposium on Steel Science. ISSS-2012, 2012, p. 187
- Suwa, Y.: Phase-field Simulation of Grain Growth. *Nippon Steel Technical Report*. (102), 19 (2013)
- Seki, A., Sawada, M., Moriguchi, K., Shirai, Y.: Simulations of Grain Growth in Titanium and Stainless Steels. *Nippon Steel & Sumitomo Metal Technical Report*. (106), 41 (2014)
- Suwa, Y.: Phase-field Simulation of Recrystallization Based on the Unified Subgrain Growth Theory. *Nippon Steel & Sumitomo Metal Technical Report*. (114), 20 (2017)
- Lindemann, F.: *Z. Phys.* 11, 609–612 (1910)
- Born, M.: *J. Chem. Phys.* 7, 591–603 (1939)
- Ostwald, W.: *Z. Phys. Chem.* 22, 289–330 (1897)
- Terasaki, H., Yamagishi, H., Moriguchi, K., Tomio, Y., Komizo, Y.: Experimental Determination of Elastic Modulus during Martensitic Transformation of Low Transformation Temperature Steel. *ISIJ International*. 51, 1566–1568 (2011)
- Terasaki, H., Yamagishi, H., Moriguchi, K., Tomio, Y., Komizo, Y.: Correlation between the Thermodynamic Stability of Austenite and the Shear Modulus of Polycrystalline Steel Alloy. *Journal of Applied Physics*. 111, 093523 (2012)
- Terasaki, H., Yamagishi, H., Moriguchi, K., Tomio, Y., Komizo, Y.: Erratum: Correlation between the Thermodynamic Stability of Austenite and the Shear Modulus of Polycrystalline Steel Alloy. *J. Appl. Phys.* 111, 093523 (2012); *Journal of Applied Physics*. 112, 079901 (2012)
- Terasaki, H., Moriguchi, K., Yamagishi, H., Komizo, Y., Tomio, Y.: On the Excess Shear Modulus in Relating to Martensitic Transformation in Steel. *Journal of Smart Processing*. 2, 128 (2013) (in Japanese)
- Fine, M.E., Brown, L.D., Marcus, H.L.: *Scr. Metall.* 18, 951–956 (1984)
- Andersen, O.K., Madsen, J., Poulsen, U.K., Jepsen, O., Kollár, J.: *Physica B+C*. 86–88, 249–256 (1977)
- Mehl, M.J., Aguayo, A., Boyer, L.L., de Coss, R.: *Phys. Rev. B*. 70, 014105 (2004)
- Grimvall, G., Magyari-Küpe, B., Ozoliņš, V., Persson, K.: *Rev. Mod. Phys.* 84, 945–986 (2012)
- Jin, Z.H., Gumbsch, P., Lu, K., Ma, E.: *Phys. Rev. Lett.* 87, 055703 (2001)
- Wills, J.M., Eriksson, O., Soderlind, P., Boring, A.M.: *Phys. Rev. Lett.* 68, 2802–2805 (1992)
- Mehl, M.J., Boyer, L.L.: *Phys. Rev. B*. 43, 9498–9502 (1991)
- Bain, E.C.: *Trans. Am. Inst. Min. Metall. Pet. Eng.* 70, 25–35 (1924)
- Kittel, C.: *Introduction to Solid State Physics*. 8th Edition. Maruzen, 2005
- Morito, S.: Effect of Alloying Elements on the Morphology of Lath Martensite. *Journal of Smart Processing*. 2, 110 (2013) (in Japanese)
- Cayron, C.: One-step Model of the Face-centred-cubic to Body-centred-cubic Martensitic Transformation. *Acta Cryst.* A69, 498–509 (2013)
- Cayron, C.: Continuous Atomic Displacements and Lattice Distortion during fcc-bcc Martensitic Transformation. *Acta Materialia*. 96, 189–202 (2015)
- Boyer, L.L.: *Acta Crystallogr. Sect. A: Found. Crystallogr.* 45, FC29 (1989)
- Mehl, M.J., Aguayo, A., Boyer, L.L., de Coss, R.: *Phys. Rev. B*. 70, 014105 (2004)
- de Waal, B.W.V.: *Acta Crystallogr. Sect. A: Found. Crystallogr.* 46, FC17 (1990)
- Mishin, Y., Farkas, D., Mehl, M.J., Papaconstantopoulos, D.A.: *Phys. Rev. B*. 59, 3393–3407 (1998)
- Vitek, V.: *Cryst. Lattice Defects*. 5, 1–34 (1974)
- Rice, J.R.: *J. Mech. Phys. Solids*. 40, 239–271 (1992)
- Nelson, D.R., Halperin, B.I.: *Phys. Rev. B*. 19, 2457 (1979)
- Dash, J.G.: *Rev. Mod. Phys.* 71, 1737–1743 (1999)
- Burakovsky, L., Preston, D.L., Silbar, R.R.: *Phys. Rev. B*. 61, 15011 (2000)
- Tsetseris, L.: *Phys. Rev. B*. 72, 012411 (2005)
- Hsueh, H.C., Crain, J., Guo, G.Y., Chen, H.Y., Lee, C.C., Chang, K.P., Shih, H.L.: *Phys. Rev. B*. 66, 052420 (2002)
- Zhang, W.: *Journal of Magnetism and Magnetic Materials*. 323, 2206–2209 (2011)
- Leung, T.C., Chan, C.T., Harmon, B.N.: *Phys. Rev. B*. 44, 2923 (1991)
- Saito, T., Furuta, T., Hwang, J.H., Kuramoto, S., Nishino, K., Suzuki, N., Chen, R., Yamada, A., Ito, K., Seno, Y., Nonaka, T., Ikehata, H., Nagasako, N., Iwamoto, C., Ikuhara, Y., Sakuma, T.: *Science*. 300, 464 (2003)
- Furuta, T. et al.: *J. Jpn. Inst. Met.* 70, 579 (2006) (in Japanese)
- Ashcroft, N.W., Mermin, N.D.: *Solid State Physics*. Philadelphia, Saunders College, 1987
- Okatov, S.V., Kuznetsov, A.R., Gornostyrev, Y.N., Urtsev, V.N., Katsnelson, M.I.: *Phys. Rev. B*. 79, 094111 (2009)
- Kürmann, F., Dick, A., Grabowski, B., Hickel, T., Neugebauer, J.: *Phys. Rev. B*. 85, 125104 (2012)
- Palumbo, M.: *Calphad*. 32, 693–708 (2008)
- Terasaki, H., Moriguchi, K., Tomio, Y., Yamagishi, H., Morito, S.: *Metall. and Mat. Trans. A*. 48, 5761 (2017)
- Wuttig, M., Liu, L., Tsuchiya, K., James, R.D.: *Journal of Applied Physics*. 87, 4707 (2000)
- Xiao, F., Fukuda, T., Kakeshita, T.: *Acta Materialia*. 61, 4044–4052 (2013)



**Koji MORIGUCHI**  
Chief Researcher, Dr.Eng.  
Mathematical Science & Technology Research Lab.  
Advanced Technology Research Laboratories  
20-1 Shintomi, Futsu City, Chiba Pref. 293-8511



**Yusaku TOMIO**  
Senior Researcher, Dr.Eng.  
Quality Control & Technical Service Div.  
Wakayama Works



**Hidenori TERASAKI**  
Professor, Dr.Eng.  
Faculty of Engineering  
Kumamoto University